Exp. Theo. NANOTECHNOLOGY 1 (2017) 145–159 https://doi.org/10.56053/1.3.145

Single walled carbon nanotubes reinforced intermetallic TiNi matrix nanocomposites by spark plasma sintering

Badis Bendjemil[1,2], *Mahiedinne Ali-Rachedi*[3], *Jamal Bougdira*[4], *Faming Zhang*[5, 6], *Eberhard Burkel*[5]

[1]LASEA, Dept of Chemistry, University of Badji-Mokhtar, 23000 Annaba, Algeria
[23]Department of Mechanical Ingeniering , University of 8 Mai 1945 Guelma, 24000 Guelma, Algeria
[3]Department of Mechanical Ingeniering, Faculty of Engineering Sciences, University of Badji-Mokhtar, Annaba, Algeria
[4]Institut of Jean Lamour, UMR 7198 CNRS - University of Lorraine, Faculty of Sciences and Technologies, BP 70239 F-54506 Vandoeuvre les NANCY cedex, France
[5]Physics of New Materials, Institute of Physics, 18055 Rostock, Germany
[6]School of Materials Science and Engineering, Southeast University, 211189 Nanjing, China
*) Email: Badis23@ymail.com

Received 19 May 2017; *Accepted* 22 July 2017; *Published* 15 Sep. 2017

We report the processing of single walled carbon nanotubes (SWCNTs) reinforced TiNi intermetallic matrix nanocomposites from Ti/Ni and SWCNTs powders using spark plasma sintering (SPS) at temperatures from 1000 °C to 1200 °C. The SWCNTs are doped into the TiNi matrix from 0.0 to 1.0 wt%. The effect of SWCNTs reinforcement contents on the relative density, phases, microstructure and microhardness of TiNi intermetallics matrix andCNTs/TiC/TiNi nanocomposites are studied. The experimental results show that the TiNi sintered at T= 1200 °C reinforced with 0.8 wt% SWCNTs has the highest Vicker's microhardness and relative density, which were HV 5.29 GPa and 96%, respectively. That can be explained by the precipitation of TiC and Ti2Ni in the matrix.This study explores the possibility of developing novel TiNi matrix nanocomposites with shape memory effect and biocompatibility.

Keywords: Intermetallic-matrix composites (IMCs); SWCNTs-reinforcement; Structural properties; Spark plasma Sintering; Nanocomposites; Mechanical properties.

1. INTRODUCTION

TiNi shape memory alloys have exceptional properties, uch as the shape memory effect, pseudoelasticity and biocompatibility, which enable them to be widely used in numerous applications [1]. Recent research works have shown that TiNi alloys exhibit better wear resistance than many conventional tribological materials due to their pseudoelasticity [2, 3]. Their rapid work hardening, good corrosion and fatigue resistance may also be beneficial [4]. Besides its equiatomic concentration, itis well known for its shape memory effect (SME). Due to its unique physical and mechanical properties at room temperature ductility, damping effect, corrosion resistance and biocompatibility, TiNi shape memory alloys can be used for biomedical applications [5, 6]. Porous TiNi-shapememory alloy has, for example, been considered as a promising biomedical material for orthopedics and bone implant surgeries in recent years [7].

A pulse current pressure sintering equipment was used for the consolidation at various sintering temperatures of TiNi alloy powder prepared by mechanical alloying [8]. A bulk Ni–Timaterial with refined microstructure was obtained by spark plasma sintering (SPS) starting from amorphous mechanically alloyed NiTi powders [9].It has also been made to develop TiNi matrix composites to further increase the wear resistance. The reinforcing phases include TiC [10], TiN [11] and precipitated Ti_2Ni [12], it is considered that the hard reinforcing phases can be used to sustain external load, while the TiNi matrix may accommodate deformation, absorb impact energy and retain hard particles.

Carbon nanotubes (CNTs) are considered to be the most effective reinforcement in metal–matrix composites for structural applications [13], [14], [15], [16], [17], [18], [19], [20] and [21] due to their extraordinary mechanical, thermal, and electrical properties and high aspect ratios. In the past, 1 vol% CNTs/TiNi composite with enhanced compressive properties and wear resistance have been fabricated by hot-press sintering [22]. The tensile properties of these CNT/TiNi composites have also been reported [23]. However, the strengthening effects of CNTs and any further effects on the shape memory of the composite have not been examined. Additionally, the five-volume ratio of the CNTs has resulted in insufficient strain for measuring the shape memory effect of the CNTs/NiTi composites.

In this paper, we describe the preparation of CNTs-reinforced TiNi matrix composites through a powder metallurgical process using CNTs, and Ni and Ti elemental powders. Spark plasma sintering (SPS), which requires a very short time to sinter metal and ceramic powders, was applied to consolidate the CNTs/TiNi composite powder at elevated temperaturesat 1000 and 1200 °C with and without addition from 0.4 to 1.0 wt% of (SWCNTs). The microstructure of each composite was observed, the density was determined, and its mechanical properties were studied. The chemical compositions (at.%) of the unreinforced specimen and matrix are designed as 50% Ti–50% Ni. Carbon nanotubes (CNTs) reinforced TiNi matrix nanocomposites were synthesized by spark plasma sintering (SPS) employing elemental powders. The phase structure, morphology and transformation behaviors were studied. Attempts have also been made to develop CNTs-TiNi matrix nanocomposites to further application in biomedical and shape memory effect. The effect of the CNTs on the mechanical properties and density of the nanocomposites was investigated.

2. EXPERIMENTAL PROCEDURE

As starting materials, commercially available powders of Ti (<45 micrometer, 99.7% purity), Ni (<10 micrometer, 99.9% purity, high purity Aldrich, Germany) were used with sizes of around 40 micrometer, respectively. The Ti, Ni and single-walled carbon nanotubes (SWCNTs with diameter < 2 nm) powders were mixed in a stoichiometric molar ratio of 1:1 with addition of SWCNTs in the range of 0.4 to 1.0 wt % by ball milling, and then dried in a vacuum. Fig.1 presented the starting sintering powder.
The mixtures were loosely compacted into a graphite die of 20 mm in diameter and sintered in vacuum (1 Pa) at various temperatures (1000–1200 °C) using an SPS apparatus (Tycho lab SINTER, FCT-HP-D5, FCT, Germany) (Fig.2, Table 1).

Table 1: Synthesis parameters of the sintered Nanocomposite TiNi/CNTs.

Samples	**T (^oC)**	**T (min)**	**Heating rate (^oC/min)**	**P (MPa)**	**50Ti-50Ni with wt% SWCNTs d=1nm**	**Current (A)**
SPS1	**1200**	**20**	**100**	**60**	**00**	**3000**
SPS2	**1200**	**20**	**100**	**60**	**0.8**	**3000**
SPS3	**1000**	**20**	**100**	**60**	**0.4**	**3000**
SPS4	**1100**	**20**	**100**	**60**	**0.0**	**3000**

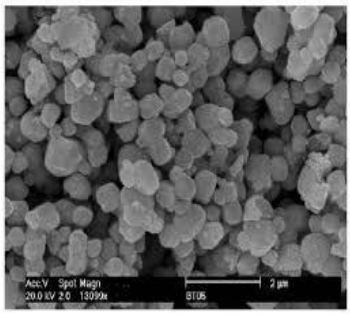

Titanium powder

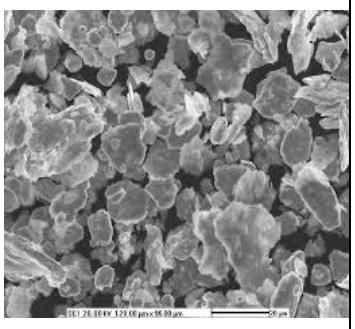

Nickel powder

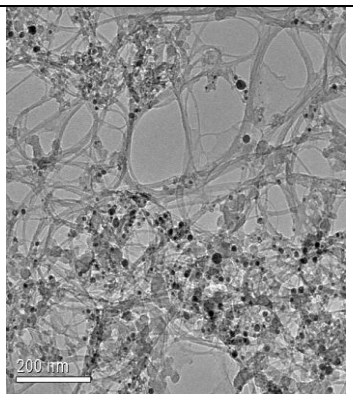

Carbon nanotubes powder

Figure 1 Starting powders before sintering.

Figure. 2. TYCHO SINTER, SPS-1050, Sumitomo Coal Mining Co. Ltd., Rostock, GERMANY.

A constant heating rate of 100 ºC/min was employed, while the applied pressure was 60 MPa. The on/off time ratio of the pulsed current was set to 12/2 in each run. The maximum current reached approximately 3000 A during sintering. The soaking time at high temperatures was within 10 min. The mixed powders used for sintering were obtained from ball milling and heterogeneous coacervation methods. The unreinforced sample and a composite with an SWCNT weight fraction of SWCNTs were fabricated by SPSat 1000, 1100 and 1200 °C under a pressure of 60 MPa and total cycle of 20 min. The sintered sample was polished and the density was determined.

The phase identification and the preferred orientation of the TiNi reinforced SWCNTs crystalline grains were evaluated by X-ray diffraction analysis by Bruker (Type D4, GmbH) using Cu Kα radiation in the angular range of 2h = 20–80 degrees at a step rate of 0.020 s to identify the crystalline phases of the sintered samples at room temperature. The morphology of the elemental powders' particles and the microstructure of the sintered specimens were determined with a scanning electron microscope (FESEMTscan Vega, GmbH). The optical and FESEM micrographs were used to determine the porosity of the sintered specimens by MIP Microstructural Analysis Processing Software. The product was cut along the cylindrical axis by Archimedes' method using water immersion. The microhardness at the top surface and the

lateral surface were measured by a diamond Vickers hardness tester. The indentation loads, ranging from 10 to 500 N, were applied for 20 s for each measurement.

3. RESULTS AND DISCUSSION

3.1. XRD analysis of powders and sintered TiNi-SWCNTs nanocomposites

Figure 3, 4, and 5 shows the XRD spectrum of the pure TiNi and the reinforced nanocomposite by SWCNTs. It can be seen that the main phase is the TiNi phase, and precipitated TiC, Ti_2Ni phases co-exist in the three samples. XRD patterns of the TiNi, and the nanocomposites are shown in Fig. 5. The Ti_2Ni phase was formed during the sintering process in all of the samples because it is a thermodynamically favorable phase at the sintering temperature compared with TiNi phase [17]:

$$Ni+Ti \rightarrow NiTi,\ \Delta G=-176.7\ kJ/mol \text{ at } 1173K \quad (1)$$

$$Ni+2Ti \rightarrow Ti_2Ni,\ \Delta G=-251.4\ kJ/mol \text{ at } 1173K \quad (2)$$

$$Ti+C \rightarrow TiC,\ \Delta G = -171.18\ kJ/mol \text{at } 1173K \quad (3)$$

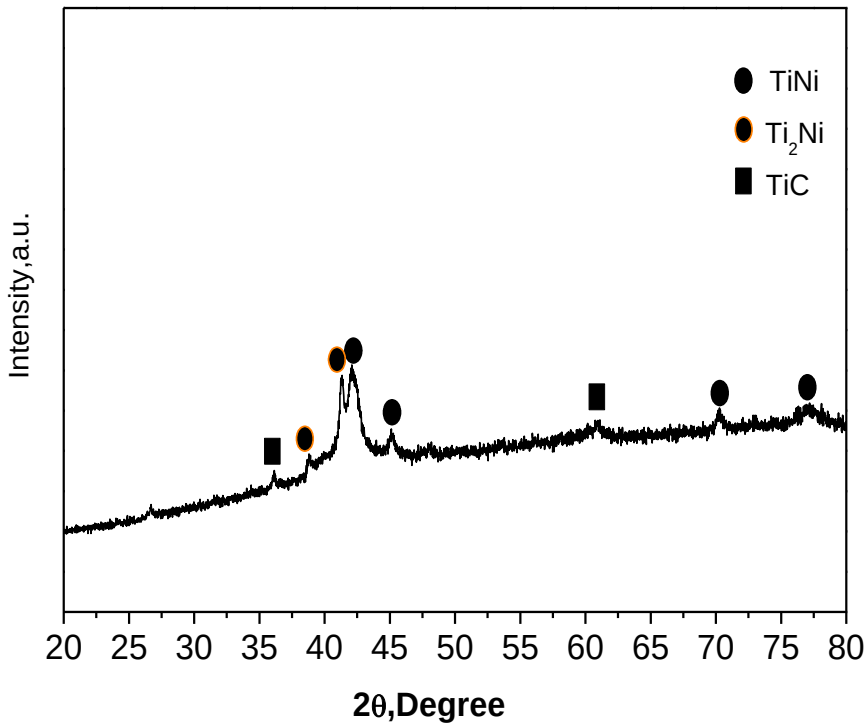

Figure. 3. XRD spectra of unreinforced TiNi sintered at T=1200°C **(SPS_1)**

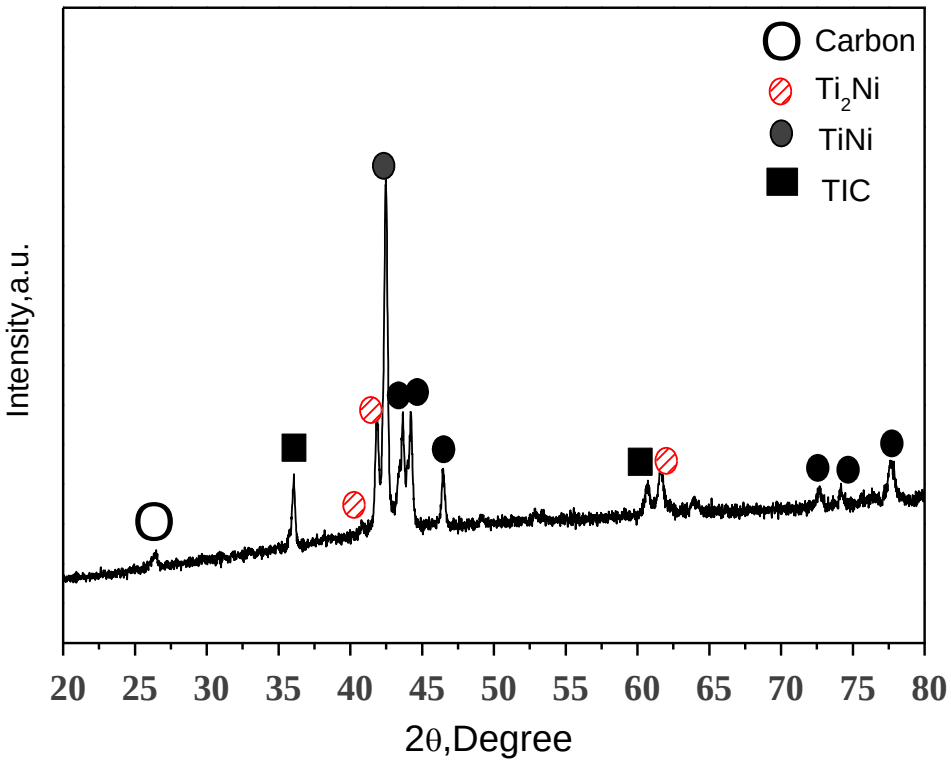

Figure. 4. XRD spectra of reinforced TiNi-CNTs nanocomposites produced at T=1200°C reinforced with 0.8 wt% SWCNTs **(SPS$_2$)**

XRD spectrum of the nanocomposite, indicates that the reaction between the Ti powders and SWCNTs did happen during the sintering process. This reaction has been previously observed [24], and it is considered that disordered carbons on wall defects and the open ends of the SWCNTs serve as carbon sources for interfacial reaction. The sintered samples consisted mainly of TiNi matrix, as major phases, and some secondary phases, such as TiC and Ti_2Ni, appeared depending on the sintering temperature. X-ray diffraction patterns of sample (0.8 Wt% CNTs-TiNi matrix nanocomposites) sintered at 60 MPa pressure were enhanced because they were reinforced with three phases, TiC, Ti_2Ni and SWCNTs with higher intensity is shown in Fig. 3, 4 and 5. Fig. 3 shows the SWCNTs content as a function of sintering temperature, which was reduced to 5 wt% when sintered at 1200 °C for 10 min at 60 MPa pressure because it reacted with Ti to produce TiC new reinforcement.

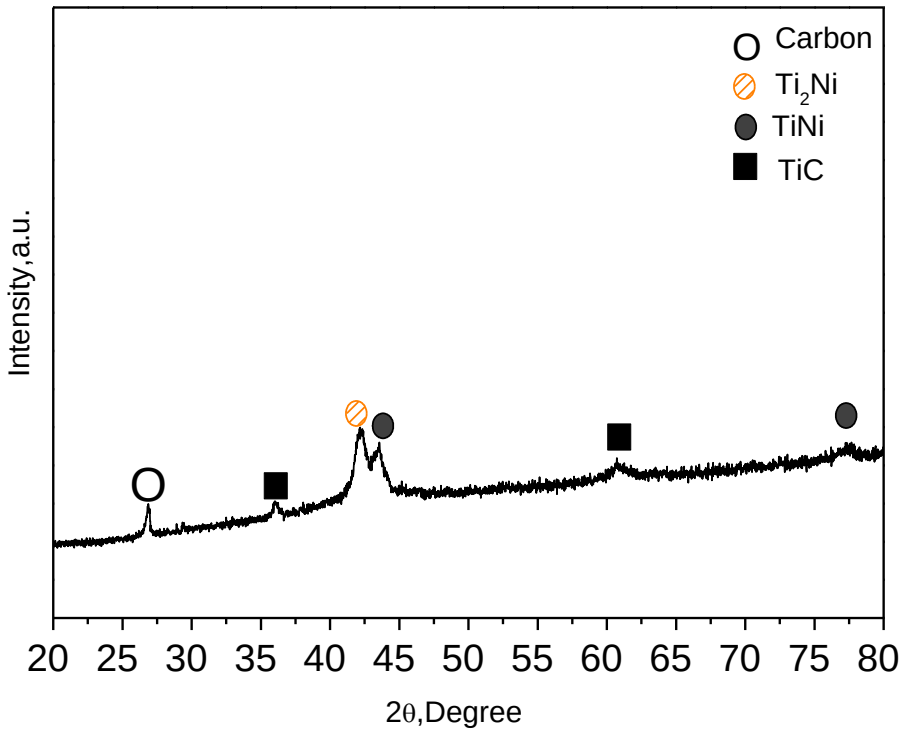

Figure. 5. XRD spectra of TiNi-CNTs nanocomposites produced at T=1000°C reinforced with 0.4 wt% SWCNTs **(SPS3)**

3.2. FESEM microstructural observation of sintered CNTs-TiNi nanocomposites

The worn surfaces and wear debris are compared in Figure 5. The Microstructuraland EDS analysis displays elemental analyses of the various regions of the sintered samples,TiNi, and the CNTs/TiC/TiNi nanocomposites in chemical composition (at.%) (Fig. 6, 7 and 8). It can be seen that, with the addition of CNTs reinforcements, the contents of Ti, Ni and O in the sintered samples decrease. According to the above results, it can be concluded that the wickers hardness has been improved by adding SWCNTs.

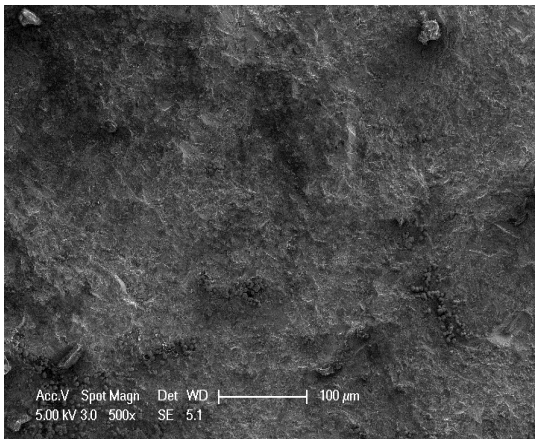
Acc.V Spot Magn Det WD 100 µm
5.00 kV 3.0 500x SE 5.1

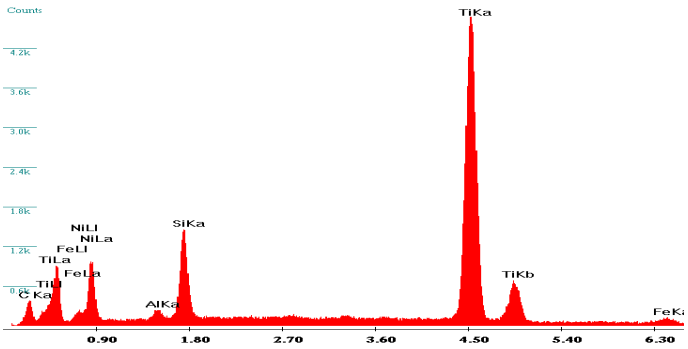
Counts
TiKa
SiKa
NiLl
NiLa
FeLl
TiLa
FeLa
TiLl
C Ka
AlKa
TiKb
0.90
1.80
2.70
3.60
4.50
5.40
6.30

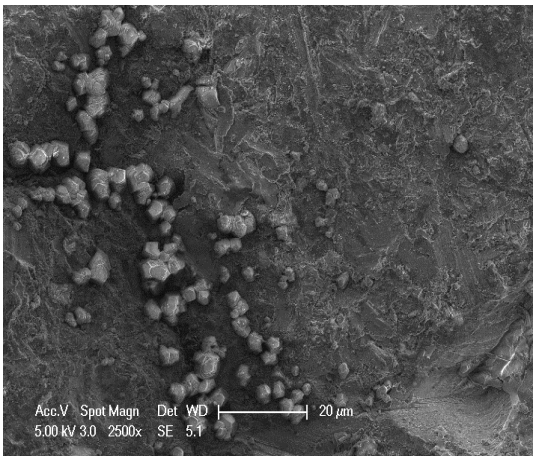
Acc.V Spot Magn Det WD 20 µm
5.00 kV 3.0 2500x SE 5.1

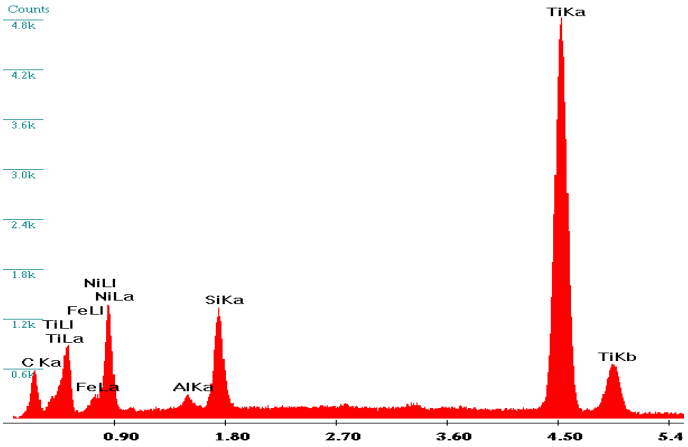
Counts
TiKa
NiLl
NiLa
FeLl
SiKa
TiLl
TiLa
C Ka
TiKb
FeLa
AlKa
0.90
1.80
2.70
3.60
4.50
5.4

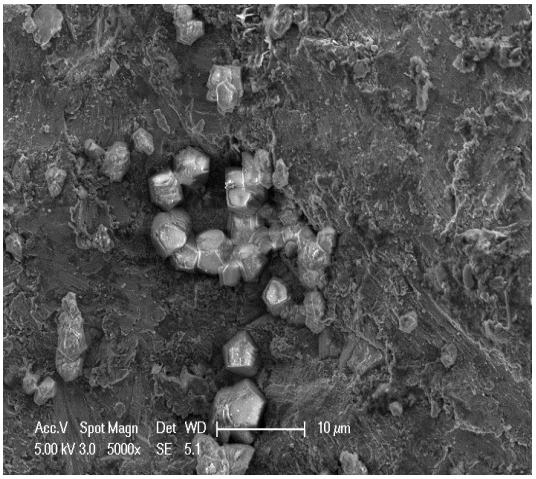
Acc.V Spot Magn Det WD 10 µm
5.00 kV 3.0 5000x SE 5.1

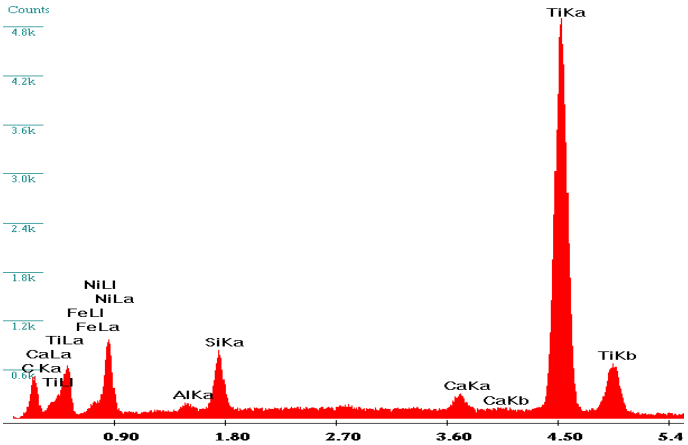
Counts
TiKa
NiLl
NiLa
FeLl
FeLa
TiLa
SiKa
CaLa
TiKb
C Ka
TiLl
CaKa
CaKb
AlKa
0.90
1.80
2.70
3.60
4.50
5.4

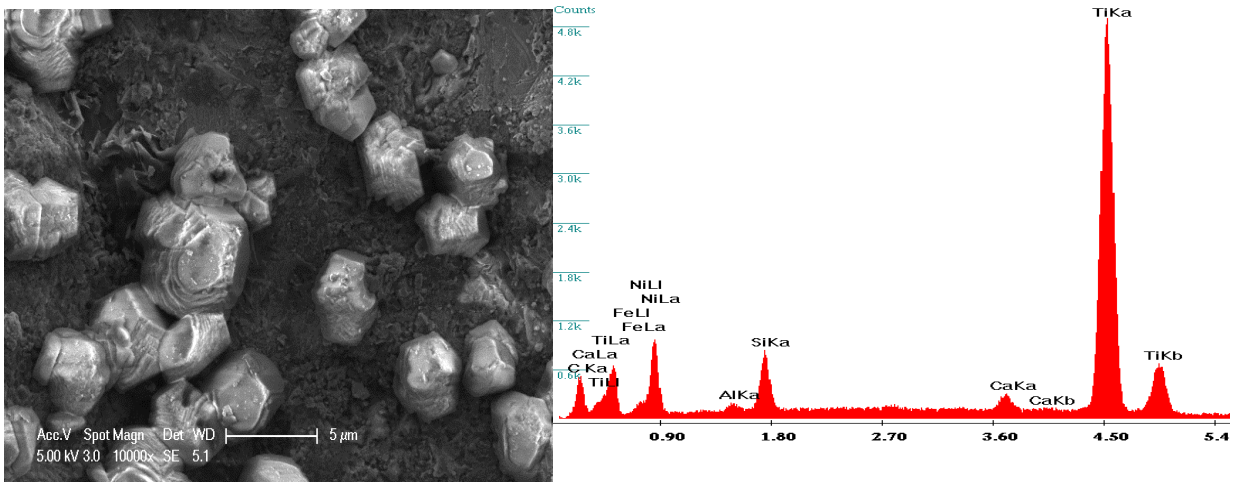

Figure. 6. Micrographs from the worn surfaces of unreinforced TiNi produced at T=1200°C

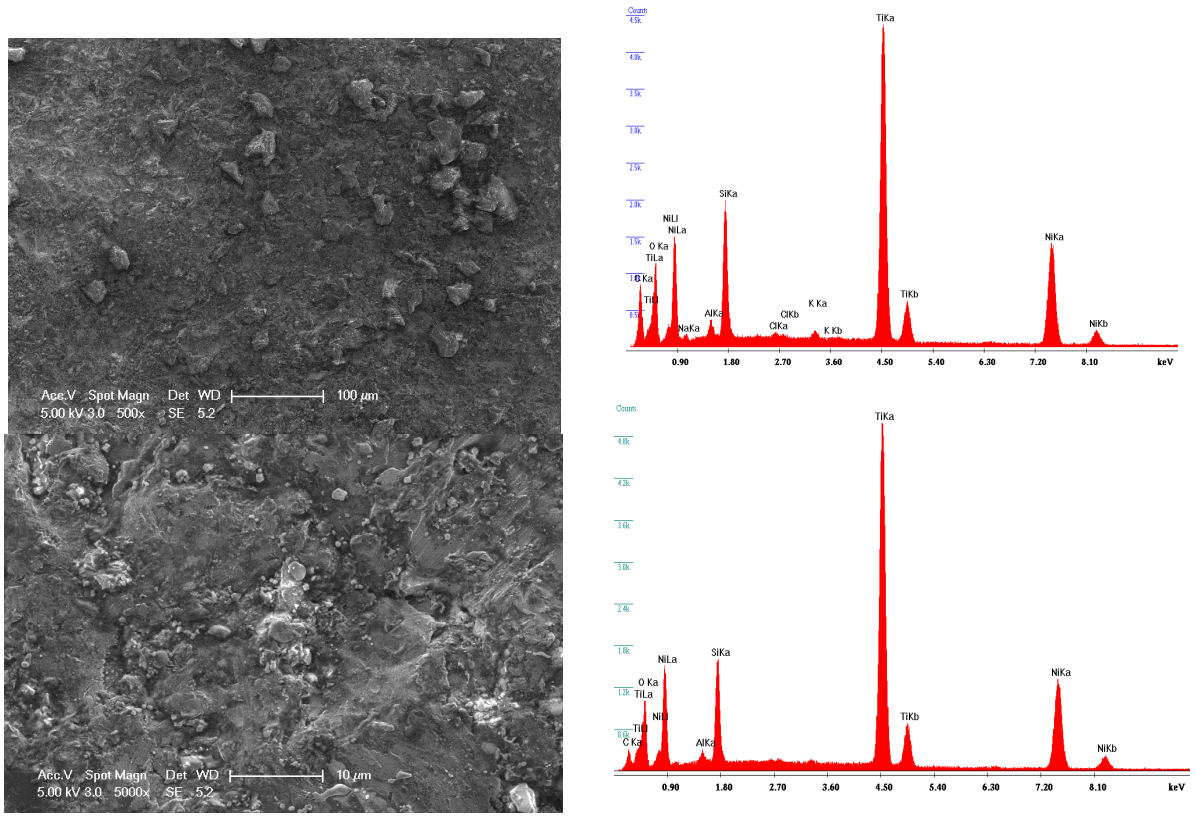

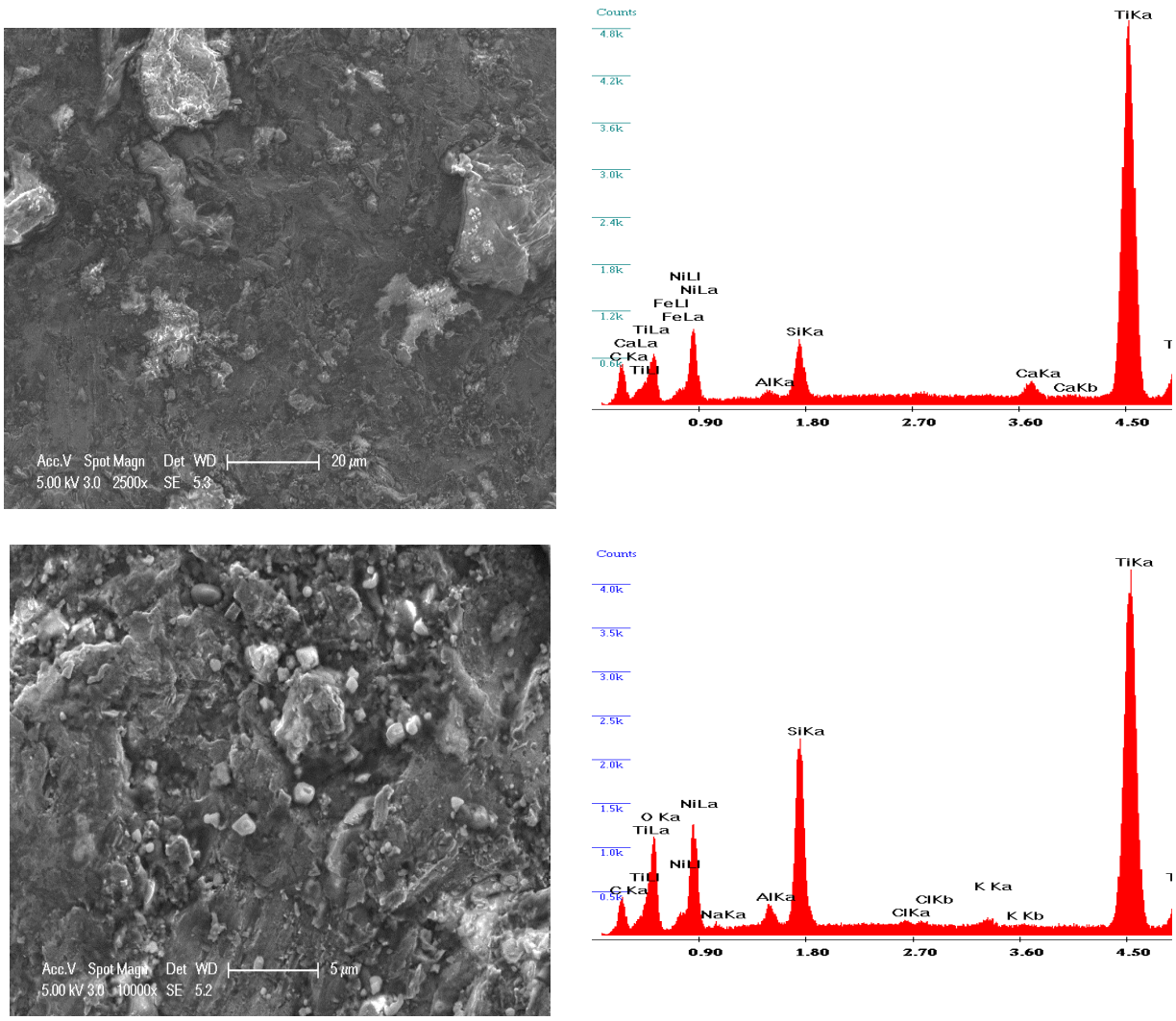

Figure. 7. FESEM micrographs from the worn surfaces of TiNi-CNTs nanocomposites produced at T=1200°C reinforced with 0.8 wt% SWCNTs

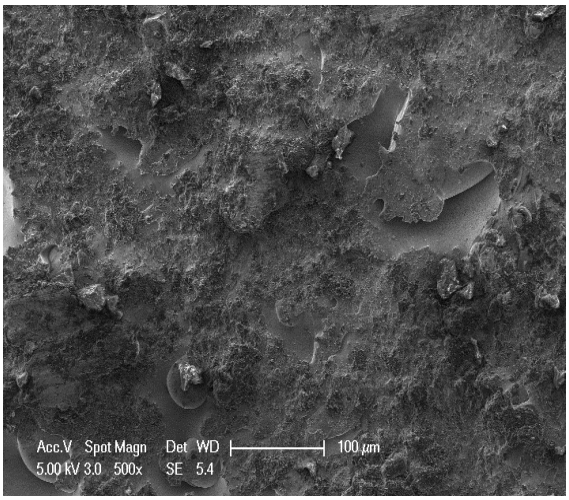
Acc.V Spot Magn Det WD 100 µm
5.00 kV 3.0 500x SE 5.4

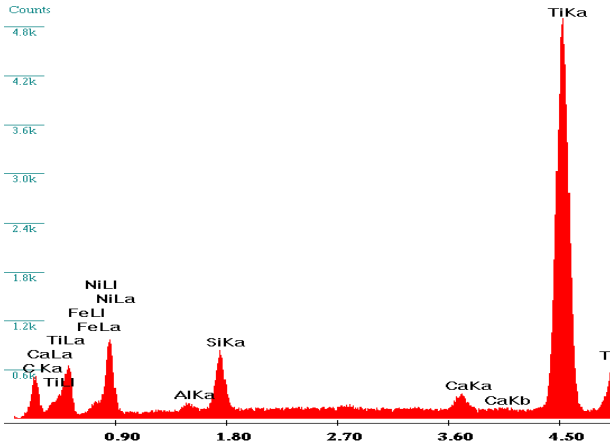
Counts
TiKa
NiLl
NiLa
FeLl
FeLa
TiLa
CaLa
C Ka
TiLl
AlKa
SiKa
CaKa
CaKb
0.90
1.80
2.70
3.60
4.50

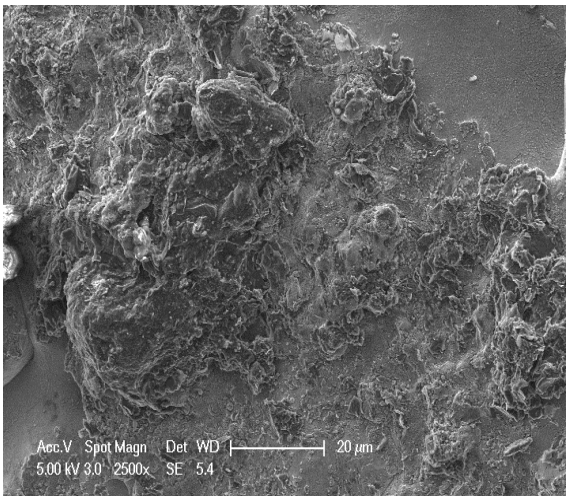
Acc.V Spot Magn Det WD 20 µm
5.00 kV 3.0 2500x SE 5.4

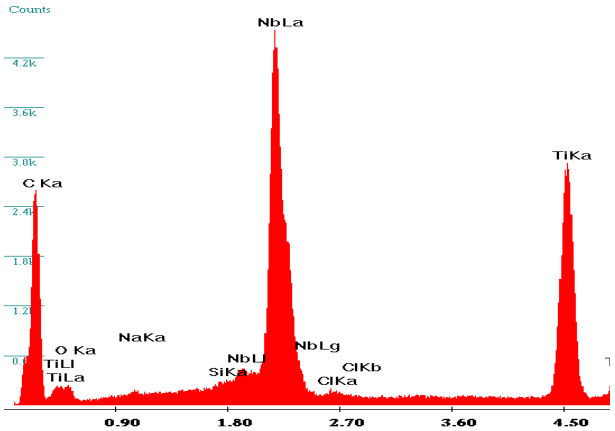
Counts
NbLa
TiKa
C Ka
O Ka
TiLl
TiLa
NaKa
NbLl
SiKa
NbLg
ClKb
ClKa
0.90
1.80
2.70
3.60
4.50

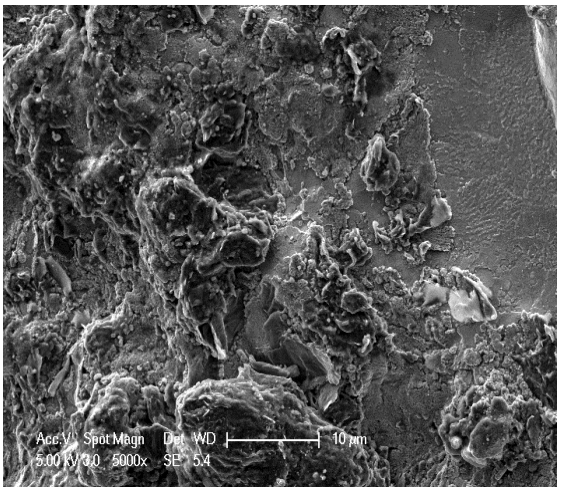
Acc.V Spot Magn Det WD 10 µm
5.00 kV 3.0 5000x SE 5.4

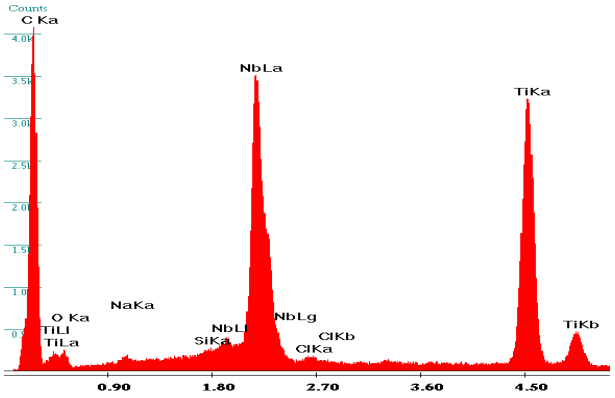
Counts
C Ka
NbLa
TiKa
O Ka
TiLl
TiLa
NaKa
NbLl
SiKa
NbLg
ClKb
ClKa
TiKb
0.90
1.80
2.70
3.60
4.50

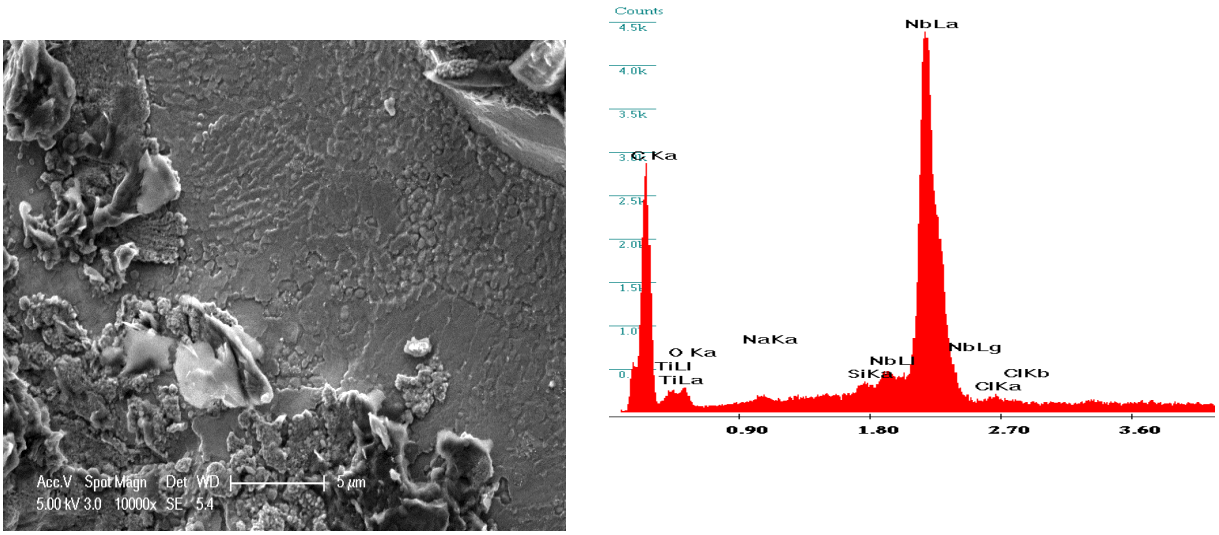

Figure. 8. FESEM micrographs from the worn surfaces of TiNi-CNTs nanocomposites produced at T=1000°C reinforced with 0.4 wt% SWCNTs

Figure. 7 shows the microstructure and the EDS spectra of the TiNi, and the CNTs/TiC/TiNi nanocomposites. EDS spectra was used to determine the elemental composition of the different regions in the sample and are presented by the red specta. The SEM micrographs in Fig. 7 shows a dark phase that corresponds to the TiNi matrix phase, and a lighter phase that corresponds to Ti_2Ni which exists mainly at the grain boundary, TiC is represented by the agglomerat in cubique polycristal form in addition to unreacted CNTs [16].

3.3. Relative density and microstructure

The variation of the relativedensity of sintred TiNi and TiNi–CNTs nanocomposites with SWCNTs reinforcement is shown in Fig. 9. The theoritical density of the composite used for obtaining relative density was calculated using a rule of mixture using the densities of two of the constituant phase (ρ_{TiNi} = 6.55 g cm^2 , ρ_{SWCNTs} = 2.25 g cm^2) with the given SPS processing paramaters, the TiNi sample exibited best densification with relative density greater than 98%, with the simlar prossessing parameters and variation of temperature CNTs–TiNi nanocomposites.

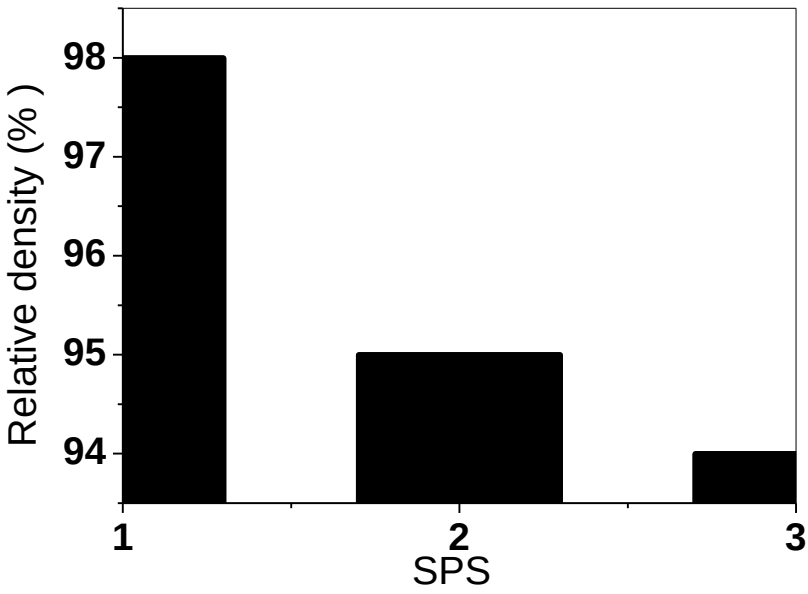

Figure. 9. Relative densities of the TiNi–CNTs nanocomposites as a function of SWCNTs reinforcement content **(SPS$_1$) (SPS$_2$) (SPS$_3$)**

The relative density decresed with incressing wt% CNTs reinforcement. The TiNi–SWCNTs nanocomposites 0.8 wt% CNTs at T=1200 °C exibited relative density of about 95%. Clearly, the CNTs reinforcement makes the densification of CNTs–TiNi nanocomposites more difficult. This seems to be the direct consequence of higher melting point of SWCNTs (T=3160 °C) compared to that of TiNi (T=3000 °C). XRD analysis indicated formation of new intermediate phase $TiNi_2$ from the action between Ti and Ni, while the intensities of SWCNTs peaks remained unchanged.

Depending on the final density to be achieved, the SPS operating condition were properly chosen, that is, 750 °C, 5 MPa for 5 min, to obtain a relative density of 75 %, 800 °C, 25 MPa for 5 min, for samples 87 % dense, and 850 °C, 50 MPa for 5 min, for zero porosity compacts. The 13% porosity sample exhibited a round microstructure with high ductility, while the 25% porous product displayed much lower stress flow as compared to that of the 13 % porosity [24**]**. Also, the easy sledding of their walls when attached by weak van der Waals force of coaleced MWCNTs can probablydecrease the relative density.

3.4. Microhardness

Fig. 10 presents the variation of Vickers microhardness of CNTs-TiNi nanocomposites with CNTs reinforcement content. The microhardness of the composites increased almost linearly with increasing SWCNTs reinforcement content. The hardness of SWCNTs (28–30 GPa) isnearly 7–8 times the previously reported values of hardness of TiNi (4 GPa). For the nearly single phase TiNi -SPS sintered in this investigation, the microhardness was found to be 5.96 GPa (measured with indentation load of 10 N), which is higher than the previously reported hardness values for monolithic [22]. While the higher hardness of the TiNi sample could be

due to minor amounts of SWCNTs phase in the TiNi sample, it could also be due to indentation size effects. It was reported that the hardness decreases with increasing load and asymptotvalue of 2 GPa at higher loads. The microhardness intherange of about 2.5–3.5 GPa

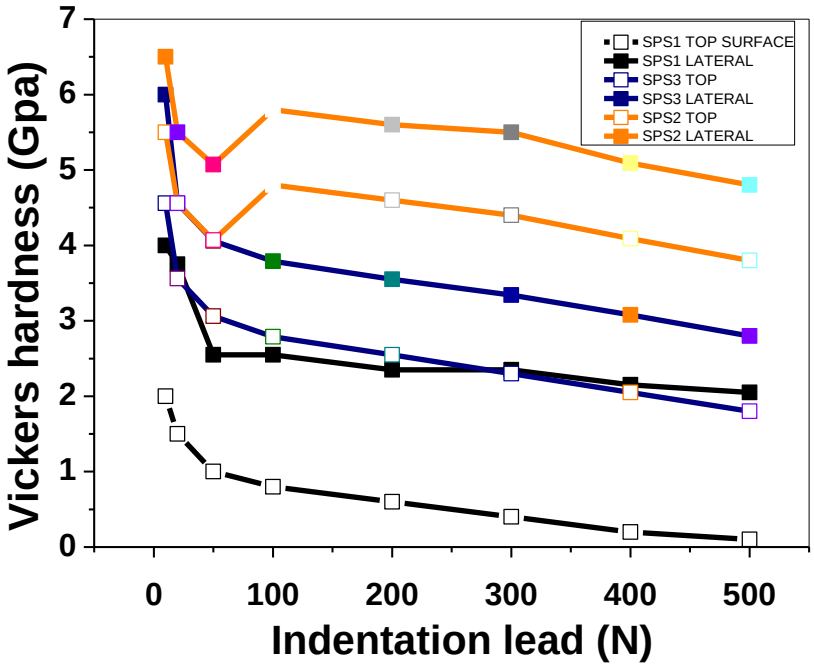

Figure. 10. Vickers microhardness of TiNi–CNTs nanocomposites as a function of SWCNTs reinforcement content **(SPS$_1$) (SPS$_2$) (SPS$_3$)**

It was found for lower loads (10 N). The TiNi–SWCNTs nanocomposites reinforced with 0.8 wt% of SWCNTs exhibited the highest hardness of about 5.5–6.5 GPa. A slight increase in average hardness have been obtained from TiNi matrix nanocomposites prepared by sintering 0.8 wt % single-walled carbon nanotubes (SWCNTs) with Ti and Ni elemental powders. It is considered that *in situ*,TiC and the remaining SWCNTs act as reinforcements and plays a major role in the improvement. Finnaly, the unreacted SWCNTs (Fig.6) coalesced to MWCNTs function of the temperature and process the highest hardness. It is believed that a large recoverable strain will lead to a low maximum contact pressure, and the deformation recovery can also diminish plastic deformation and retard crack propagation, thus minimizing the surface damage [18]. The formation of TiC is functionof the tempetature and CNTs reinforcement as carbon source. Also, the improvement of compressive mechanical and tribo nanocomposite, properties will be tested. The memory effect and bionanocomposite compitability will also be performed in the near future.

3. CONCLUSIONS

Dense CNTs–TiNi nanocomposites with varying weight fraction of coated CNTs were fabricated successfully by SPS in the range of 1000, 1100, and 1200 °C under a pressure of 60 MPa for 20 min in pure Ar atmosphere protection. The TiNi with 0.8 wt% SWCNTs had the

highest Vicker's microhardness and relative density, which were HV 5.29 GPa and 96%, respectively. This increased with the addition of CNTs. Although TiC was formed by reaction of CNT and Ti, unreacted CNTs could be found. Mechanical properties of TiNi were enhanced by unreacted CNTs.

Acknowledgements

We are grateful to Prof. Jaafar Gambaja, Drs. Damien Genève and Ghouti Medjeldi (Institut Jean Lamour, University of Henri Point Carré, Nancy, France) for the help in FESEM and XRD investigations.

References

[1] T. Duerig, A. Pelton, D. Stockel. Mater Sci Eng A 273–275 (1999) 149
[2] N.B. Morgan Mater Sci Eng A 378 (2004) 16
[3] Kujala Sauli. Biocompatibility and biomechanical aspects of nitinol shape memory metal implants. Finland: Department of Surgery, Department of Anatomy and Cell Biology, University of Oulu press; (2003)
[4] K. Otsuka, X. Ren, Progress in Materials Science 50 (2005) 511
[5] M. Abedini, H.M. Ghasemi, M.N. Ahmadabadi, Materials Characterization 61 (2010) 689
[6] M. Abedini, H.M. Ghasemi, M.N. Ahmadabadi, Materials Science and Technology 26 (2010) 285
[7] Y. Shida, Y. Sugimoto, Wear 146 (1991) 219
[8] L. L. Ye, Z.G. Liu, K. Raviprasad, M. X. Quan, M. Umemoto, Z.Q. Hu, Mater. Sci. Eng.A 241 (1998) 290
[9] A. Teray ama, H. Kyogoku, M. Sakamura, S. Komatsu, Mater. Trans. 47 (2006) 550
[10] H.Z. Ye, R. Liu, D.Y. Li, R. Eadie, Scripta Mater., 41 (1999) 1039
[11] Y.C. Luo, D.Y. Li, Journal of Materials Science, 36 (2001) 4695
[12] X. Hu[a], Y.F. Zheng, Y.X. Tong, F. Chen, B. Tian, H.M. Zhou, L. Li, Materials Science and Engineering: A 623 (2015) 1
[13] T. Kuzumaki, K. Miyazawa, H. Ichinose, K. Ito, J. Mater. Res., 13 (1998) 2445
[14] H. Kwon, M. Estili, K. Takagi, T. Miyazaki, A. Kawasaki, Carbon, 47 (2009) 570
[15] W.A. Curtin, B.W. Sheldon, Mater. Today 7 (2004) 44
[16] E.T. Thostenson, Z.F. Ren, T.W. Chou, Compos. Sci. Technol., 61 (2001) 1899
[17] W.X. Chen, J.P. Tu, L.Y. Wang, H.Y. Gan, Z.D. Xu, X.B., Zhang Carbon, 41 (2003) 215
[18] S.I. Cha, K.T. Kim, S.N. Arshad, C.B. Mo, S.H. Hong, Adv. Mater., 17 (2005) 1377
[19] D.H. Nam, S.I. Cha, B.K. Lim, H.M. Park, D.S. Han, S.H. Hong, Carbon, 50 (2012) 2417
[20] K.T. Kim, S. Il Cha, S.H. Hong, S.H., Mater. Sci. Eng. A – Struct., 430 (2006) 27
[21] Y.J. Jeong, S.I. Cha, K.T. Kim, K.H. Lee, C.B. Mo, S.H., 3 (2007) 840
[22] X. Feng, J.H. Sui, W. Cai, A.L. Liu, Scr. Mater., 64 (2011) 824
[23] X. Feng, J.H. Sui, W. Cai, J. Compos. Mater., 45 (2011) 1553
[24] Yeon-wook Kim , Materials Letters162 (2016) 1